Burns & Trauma, 2025, **13**, tkae071
https://doi.org/10.1093/burnst/tkae071
Research Article

OXFORD

Exosomes derived from fibroblasts enhance skin wound angiogenesis by regulating HIF-1α/VEGF/VEGFR pathway

Yunxia Chen[1,2], Wenjing Yin[1,2], Zhihui Liu[1,2], Guang Lu[3,4], Xiaorong Zhang[1,2], Jiacai Yang[1,2], Yong Huang[1,2], Xiaohong Hu[1,2], Cheng Chen[1], Ruoyu Shang[1], Wengang Hu[1], Jue Wang[1], Han-Ming Shen[4,5], Jun Hu[6,*], Gaoxing Luo[1,2,*], Weifeng He[1,2,*]

[1]State Key Laboratory of Trauma, Burn and Combined Injury, Institute of Burn Research, Southwest Hospital, Third Military Medical University (Army Military Medical University), Gaotanyan street, Shapingba district, Chongqing 400038, China
[2]Chongqing Key Lab for Wound Repair and Tissue Regeneration, Southwest Hospital, Third Military Medical University (Army Military Medical University), Gaotanyan street, Shapingba district, Chongqing 400038, China
[3]Zhongshan School of Medicine, Sun Yat-sen University, Zhongshan second road, Yuexiu district, Guangzhou 510062, China
[4]Department of Physiology, Yong Loo Lin School of Medicine, National University of Singapore, 21 Lower Kent Ridge Road, Singapore 119077, Singapore
[5]Faculty of Health Sciences, Ministry of Education Frontiers Science Center for Precision Oncology, University of Macau, Macao Taipa University Avenue, Macau 999078, China
[6]Department of Neurology, Southwest Hospital, Third Military Medical University (Army Military Medical University), Gaotanyan street, Shapingba district, Chongqing 400038, China

*Corresponding authors. Jun Hu, E-mail: hujun@tmmu.edu.cn; Gaoxing Luo, E-mail: logxw@yahoo.com and Weifeng He, E-mail: heweifeng@tmmu.edu.cn

Abstract

Background: Angiogenesis is vital for tissue repair but insufficient in chronic wounds due to paradoxical growth factor overexpression yet reduced neovascularization. Therapeutics physiologically promoting revascularization remain lacking. This study aims to investigate the molecular mechanisms underlying fibroblast-derived exosome-mediated angiogenesis during wound repair.
Methods: To assess the effects of fibroblasts derived exosomes on wound healing and angiogenesis, a full-thickness mouse skin injury model was established, followed by pharmacological inhibition of exosome secretion. The number and state of blood vessels in wounds were assessed by immunofluorescence, immunohistochemistry, hematoxylin–eosin staining, and laser Doppler imaging system. The high-throughput miRNA sequencing was carried out to detect the miRNA profiles of fibroblast-derived exosomes. The roles of candidate miRNAs, their target genes, and relevant pathways were predicted by bioinformatic online software. The knockdown and overexpression of candidate miRNAs, co-culture system, matrigel assay, pharmacological blockade, cell migration, EdU incorporation assay, and cell apoptosis were employed to investigate their contribution to angiogenesis mediated by fibroblast-derived exosomes. The expression of vascular endothelial growth factor A (VEGFA), vascular endothelial growth factor receptor 2 (VEGFR2), hypoxia-inducible factor 1α (HIF-1α), von Hippel–Lindau (VHL), and proline hydroxylases 2 was detected by western blot, co-immunoprecipitation, immunofluorescence, real-time quantitative polymerase chain reaction, flow cytometry, and immunohistochemistry. Furthermore, a full-thickness mouse skin injury model based on type I diabetes mellitus induced by streptozotocin was established for estimating the effect of fibroblast-derived exosomes on chronic wound healing.
Results: Pharmacological inhibition of exosome biogenesis markedly reduces neovascularization and delays murine cutaneous wound closure. Topical administration of fibroblast-secreted exosomes rescues these defects. Mechanistically, exosomal microRNA-24-3p suppresses VHL E3 ubiquitin ligase levels in endothelial cells to stabilize hypoxia-inducible factor-1α and heighten vascular endothelial growth factor signaling. MicroRNA-24-3p-deficient exosomes exhibit attenuated pro-angiogenic effects. Strikingly, topical application of exosomes derived from fibroblasts onto chronic wounds in diabetic mice improves neovascularization and healing dynamics.
Conclusions: Overall, we demonstrate central roles for exosomal miR-24-3p in stimulating endothelial HIF-VEGF signaling by inhibiting VHL-mediated degradation. The findings establish fibroblast-derived exosomes as promising acellular therapeutic candidates to treat vascular insufficiency underlying recalcitrant wounds.

Received: May 5, 2024. **Revised:** October 19, 2024. **Accepted:** October 30, 2024
© The Author(s) 2025. Published by Oxford University Press.
This is an Open Access article distributed under the terms of the Creative Commons Attribution Non-Commercial License (https://creativecommons.org/licenses/by-nc/4.0/), which permits non-commercial re-use, distribution, and reproduction in any medium, provided the original work is properly cited. For commercial re-use, please contact journals.permissions@oup.com

Downloaded from academic.oup.com/burnstrauma/article/doi/10.1093/burnst/tkae071/8151405 by guest on 13 October 2026

Graphical Abstract

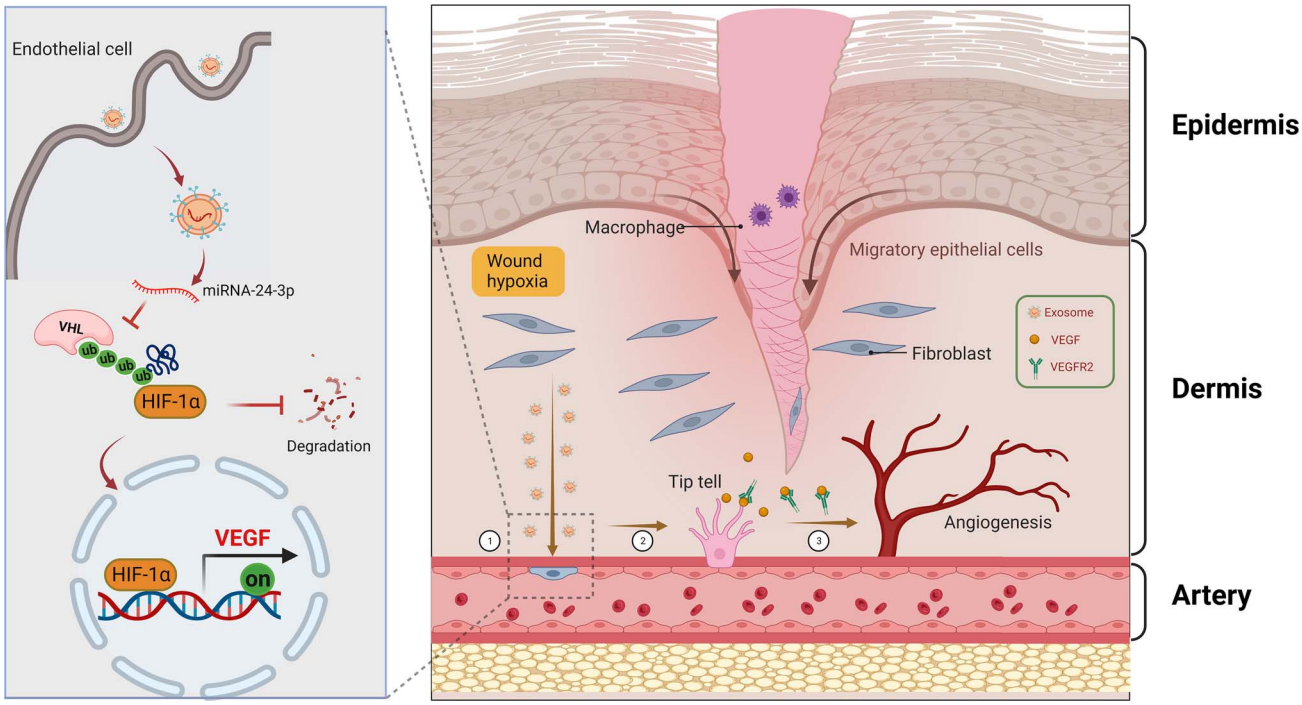

Keywords: Fibroblasts; Exosomes; Angiogenesis; Wound healing; MicroRNA-24-3p

Highlights

- By conditionally inhibiting endogenous exosome biogenesis, we provide direct genetic evidence positioning fibroblast-secreted exosomes as indispensable paracrine effectors orchestrating multicellular crosstalk governing physiological angiogenesis.
- Through unbiased sequencing coupled with functional validations, we identify exosome-transferred microRNA-24-3p as a vital genetic cargo that enhances HIF-1α stability by suppressing VHL in recipient endothelial cells.
- We delineate the activation of VEGF–VEGFR2 master signaling cascade, underlying fibroblast exosome stimulated proliferation, migration, and tubulogenesis of endothelial cells.
- As compelling proof-of-concept of translational potential, we demonstrate simply topical application of fibroblast exosomes can effectively rescue severely impaired vascularization within ischemic chronic wounds in murine diabetic models.

Background

The formation of new blood vessels from pre-existing vasculature, termed angiogenesis, is vital for the development, tissue growth, and homeostatic repair [1–4]. This complex multistep process encompasses endothelial tip cell selection, sprout formation, extracellular matrix (ECM) degradation, proliferation, anastomosis, and lumenization to establish perfused neovessels [5–7]. Physiologically, angiogenesis is transiently activated by tissue injury and hypoxia to enable regenerative responses [8]. However, in chronic diseases such as diabetes, the revascularization is paradoxically insufficient despite the heightened growth factor expression, contributing to the pathogenesis of non-healing wounds, ulcers, and gangrene [9–11]. Hence, the therapeutic approaches to stimulate neovascularization remain much sought after in regenerative medicine.

Angiogenesis requires the intricate spatiotemporal interplay between responsive endothelium and activating perivascular cells such as fibroblasts. In addition to endothelium-intrinsic vascular endothelial growth factor (VEGF) signaling, stromal cells secreting pro-angiogenic growth factors (GFs) and cytokines stereotypically stimulate tip cell selection, migration, and proliferation [1,5,8]. Fibroblasts adjacent to microvessels represent a predominant source of these stimuli during the development and wound repair [5,12]. Reciprocally, endothelial-secreted platelet-derived growth factor and transforming growth factor-β induce myofibroblast differentiation to facilitate the maturation of newly formed vessels [12]. Hence, angiogenesis entails interdependent heterocellular communication.

Exosomes have recently emerged as critical regulators to facilitate complex heterocellular crosstalk [13]. These nano-sized extracellular vesicles that originated from endosomal compartments mediate intercellular transfer of bioactive proteins and genetic material. Exosomes reprogram cellular behavior by modulating signaling, gene expression, and metabolism in recipient cells [14,15]. All cells constitutively release exosomes, whose secretion is enhanced upon activation [14,16]. Importantly, exosomal cargo reflects and transfers the physiological state of parent cells. Hence, in addition to serving as biomarkers, exosomes act as endogenous mediators of tissue repair that may be therapeutically harnessed.

Pro-angiogenic effects of endothelial-derived exosomes that stimulate endothelial sprouting while suppressing macrophage infiltration to enable vascular anastomosis

Downloaded from academic.oup.com/burnstrauma/article/doi/10.1093/burnst/tkae071/8151405 by guest on 13 October 2026

were among the first documented [17]. Tumor-secreted exosomes also activate angiogenic pathways in endothelium to enhance the perfusion [18]. Bone marrow myeloid cells release exosomes that mobilize VEGF-mediated angiogenesis during wound healing and ischemia [19]. Hence, exosomes govern tissue-specific angiogenesis programs by orchestrating complex heterocellular communication [14,16,20]. However, exosomal components' specific identities and functionality mediating these effects remain largely undefined. Elucidating mechanisms underlying exosome bioactivity would enable further translational developments around acellular extracellular vesicle–based therapeutics.

In cutaneous wound healing, fibroblasts adjacent to the microvasculature activate upon hypoxic and inflammatory signaling during the proliferative phase [21,22]. They prominently regulate the endothelial behavior in paracrine, with crosstalk governing angiogenesis and consequent tissue regeneration [23]. Fibroblast-secreted products stimulate endothelial cell invasion, tubulogenesis, and vessel stabilization in vitro [24–26]. *In vivo*, evidence directly demonstrating functional roles for fibroblast-derived exosomes in activating angiogenesis remains lacking [27–29]. Defining mechanisms by which fibroblast exosomes modulate endothelial behavior would provide mechanistic insights into heterocellular communication, enabling vascularization.

Impaired angiogenesis underlies the pathogenesis of chronic non-healing wounds in diabetes, venous stasis, and ischemia [10]. Neovascularization defects arise due to intrinsically poor ECM, nerve damage, and infection beyond insufficient GFs [30]. Promoting revascularization using recombinant proteins or gene therapy in preclinical models enhances the healing of these recalcitrant wounds [9,11]. However, the direct administration of recombinant GFs possesses drawbacks, including the need for repeated applications, poor bioavailability, and off-target effects [31]. Cell-based therapy using endothelial progenitors or fibroblasts also stimulates neovascularization but suffers challenges in optimization, scale-up, regulation, and clinical translation [11,32].

Hence, the acellular vesicular therapy utilizing endogenous exosomes to stimulate angiogenesis physiologically represents an attractive translational approach. Fibroblast exosomes capable of enhancing revascularization could overcome current limitations in protein/gene/cell therapies. However, their therapeutic efficacy and mechanisms of action remain to be systematically evaluated. Elucidating mechanisms governing exosome-mediated regulation of angiogenesis would propel the development of acellular extracellular vesicle–based therapeutics.

In this study, we demonstrate the indispensable roles of fibroblast-secreted exosomes in activating VEGF-dependent angiogenic pathways during cutaneous wound healing. We reveal that exosomal delivery of miR-24-3p as a vital mechanism suppresses endothelial von Hippel–Lindau (VHL) to enhance HIF-1α stability and VEGF signaling. Topical administration of FB-Exos rescues deficient neovascularization in diabetic wounds. Our findings establish fibroblast exosomes as promising acellular therapeutic candidates to treat vascular insufficiency in chronic wounds and ischemic diseases.

Methods

Primary cell isolation and culture

Dermal fibroblasts were obtained from the skin of newborn (0–2 days old) mice. First, the mouse skin was incubated in a 0.25% dispase II solution (04942078001; Roche) to separate the epidermis and dermis at 4°C overnight. Then, the dermis layer was fully separated from the skin. The obtained dermis was digested with 0.25% trypsin (Hyclone) for 30 min at 37°C to generate single cell solution. Cells were seeded into culture dish at a density of 1×10^5 cells/cm^2, and expanded in Dulbecco's Modified Eagle Medium (DMEM) supplemented with 1% streptomycin/penicillin (Hyclone) and 10% exosome-free fetal bovine serum (FBS; VivaCell) at 37°C with 5% CO_2. The morphology and number of primary fibroblasts were observed under a microscope and the purity of passage 2 fibroblasts was determined by flow cytometry (Supplementary Figure 1a–c). The Animal Ethics Committee of the Third Military Medical University approved all protocols involving animal experiments. Mouse brain microvessel endothelial cells (vECs, CRL-2299) were obtained from American Type Culture Collection and cultured in DMEM supplementing with 10% FBS (Gibco) and 1% streptomycin/penicillin at 37°C with 5% CO_2. All cells tested negative for mycoplasma contamination were further used for experiments.

Isolation, identification, and label of exosomes

After 48 h of culture, the FB culture medium was harvested and centrifuged at 300×*g* and 3000×*g* at 4°C for 10 min to eliminate residual cell debris. The collected medium was centrifuged at 10 000×*g* at 4°C for 30 min to remove the remaining macropolymers. The supernatant was further ultracentrifuged at 100 000×*g* at 4°C for 70 min. The pellets were resuspended in 1× ice-cold phosphate-buffered saline (PBS) solution, ultracentrifuged at 100,000×*g* for 70 min at 4°C to remove residual contaminant proteins, and then dissolved in 1× ice-cold PBS for analysis. For exosome characterization, the harvested exosomes were quantified using a bicinchoninic acid (BCA) protein assay kit (R33200; Thermo Fisher, USA) for further experiments. Nanoparticle tracking analysis (DLS, Zetasizer Nano; Malvern Instruments, UK), transmission electron microscopy, CD63, TSG101, and calcein were used to identify the exosomes obtained from western blotting (Supplementary Figure 1d–f).

In some experiments, FB-Exos were fluorescently labeled by adding DiI dye (1:400, cell membrane red fluorescent probe) (Beyotime) during the ultracentrifugation step. Unbound dye was removed by additional centrifugation at 100,000×*g* for 90 min and washing in PBS. The labeled exosomes were resuspended in PBS at 10^8–10^9 particles/mL and quantified via NanoSight analyses.

To inhibit exosome genesis, fibroblasts were pre-treated with 10 μM GW4869 or vehicle control (DMSO) for 48 h during conditioned media collection. Cell viability and metabolic activity remained comparable to those of the controls upon GW4869 treatment, as ascertained by trypan blue dye exclusion and CCK8 assays, respectively.

Knockdown and overexpression of miR-24-3p

The miR-24-3p inhibitor/mimics or negative controls were purchased from GenePharma Co. Lentiviral vectors encoding miRZip antisense miRNA inhibitors or miRVec sense miRNA sequences (SBI Biosciences) were utilized to suppress or overexpress miR-24-3p in fibroblasts, respectively. Non-targeting vectors served as controls. Briefly, early passage low-density fibroblasts were transduced via polybrene-assisted spinoculation and selected with puromycin to establish stable pools with miR-24-3p knockdown or overexpression relative

Downloaded from academic.oup.com/burnstrauma/article/doi/10.1093/burnst/tkae071/8151405 by guest on 13 October 2026

to the controls. The complete medium was replaced 24 h post-infection, and the miR-24-3p levels were ascertained via quantitative polymerase chain reaction (qPCR) of isolated total RNA. Exosomes derived from FBs overexpressing miR-24-3p were referred to as $Exo^{miR\text{-}24\text{-}3p\ OE}$, whereas exosomes derived from FBs with knocked down miR-24-3p were referred to as $Exo^{miR\text{-}24\text{-}3p\ KD}$. Exosomes derived from FBs expressing miR-24-3p control vectors were referred to as $Exo^{miR\text{-}24\text{-}3p\ Ctrl}$.

Dual-luciferase reporter assay

Briefly, 1×10^4/well 293T cells with a wild-type (WT) or mutational 3′-UTR of VHL (MUT) were seeded and cultured in a 96-well plate. After adhesion, the luciferase reporter vector combined with the mimic negative control vehicle (mimics NC) or the mmu-miR-24-3p mimic was co-transfected into a monolayer of WT or mutational 293T cells for 24 h. Luciferase activity was measured under a microplate reader (Thermo, USA) via a dual-luciferase reporter assay system (Promega, USA) to analyze the binding between miR-24-3p and the 3′-UTR of VHL.

High-throughput miRNA sequencing

The total miRNAs derived from purified FB-Exos were extracted using a miRNA isolation kit (Thermo, USA). The high-throughput miRNA sequencing was carried out by the SEQHEALTH company (Wuhan, China). The total miRNA detection, the construction of gene library, and HiSeq/MiSeq sequencing were performed according to the manufacturer's instructions.

Matrigel assays

In vitro capillary network formation by vECs was detected via tube formation assay with Matrigel (BD, USA). Briefly, Matrigel was diluted 1:1 with DMEM on ice for angiogenesis experiments. A total of 70 μL of diluted Matrigel was added to a 96-well plate and incubated for 30 min at 37°C. vECs were pre-stained with calcein reagent at a ratio of 1:1000 at 37°C for 20 min, followed by two washes with 1× PBS. Subsequently, 1.5×10^4 vECs/well were seeded on Matrigel and co-cultured with 1.5×10^4/well FBs in a contact or non-contact manner without or with a 0.4-μm transwell insert. For exosome stimulus experiments, 1.5×10^4 vECs seeded on Matrigel/well were incubated with 50 μg/mL FB-Exos or HFB-Exos. After co-incubation for 6 h, the formation of vEC tube-like structures was observed under a confocal microscope, and the total length of the tube-like structure and the number of branches were calculated via ImageJ software.

EdU assays

vECs were treated with 50 μg/mL FB-Exos or HFB-Exos for 24 h. Before harvesting samples, vECs were treated with 10 μM EdU for 6 h, fixed in 4% paraformaldehyde, permeabilized using 0.5% Triton X-100 (Beyotime), and stained with Alexa Fluor azide to detect incorporated EdU by copper-catalyzed click reaction as per manufacturer's protocols (Beyotime). Cell nuclei were counterstained with 1× Hoechst 33342 and EdU+ proliferating cells enumerated. Images were obtained under a laser scanning confocal microscope (Olympus).

Cell migration

For scratch wound healing assays, the confluent vECs monolayers seeded in 12-well plates were scratched using 200-μL pipet tips to induce linear cell-free wounds ~1 mm in width. vECs were then incubated with 50 μg/mL FB-Exos for 24 h. Wound closure due to directional migration was monitored by phase contrast imaging over 24 h. Cell debris was washed away before imaging. Wound width was measured at three positions per scratch at indicated time points using NIH ImageJ software.

Cell invasion

Growth factor–reduced Matrigel was applied to the membranes of transwell inserts (8 μm pore size) in 24-well plates for 1 h at 37°C for solidification (Corning). Then, 25 000 vECs were seeded per insert in the serum-free media above wells containing 10% serum-supplemented media with or without exosomes. The cells invading through the Matrigel and the pores to the underside of the membranes over 24 h were stained with 1× crystal violet for counting via a light microscopy.

Type I diabetic mouse model

Briefly, a type I diabetic mouse model was induced in 8-week-old male C57BL/6 mice by intraperitoneal injection of streptozotocin (75 mg/kg; Sigma-Aldrich) dissolved in citrate buffer daily for 5 days. Blood glucose was measured using a glucometer test strip (Ascencia Elite; Bayer) 3 days after the last injection. Mice exhibiting hyperglycemia (>250 mg/dL glucose) were included as models of type I diabetes (T1D). The mice were maintained for 2 weeks to induce chronic complications of hyperglycemia before the wounding experiments described above. Subcutaneous blood flow in the skin of diabetic mice was measured via laser Doppler imaging to ascertain the development of circulatory deficits compared with that in the skin of age-matched normoglycemic controls as described earlier. FB-Exo therapy was administered thrice weekly to T1D mice. A total of 100 μL of PBS containing 40, 80, 200, or 400 μg of FB-Exos was subcutaneously injected into the wounds. The control mice were subcutaneously injected with an equal volume of PBS. Wound healing and quantitative angiogenesis analyses were conducted as described for the control mice above.

Full-thickness excision wound model and treatment

Sex- and age-matched C57BL/6 (C57) mice (male, specific pathogen-free, 6 weeks old) were purchased from the Animal Institutes of the Third Military Medical University for all animal experiments. The mice were anesthetized with 1% pentobarbital (Sigma, USA) (0.5–1.0 mL/100 g body weight) and their hair was shaved before the experiment. After disinfection with 75% alcohol, two full-thickness excisional wounds (6, 8, and 10 mm in diameter) were made on either side of the dorsal skin. For normal C57BL/6 mice, 50 μL of drug-loaded (0.1% DMSO) PBS, GW4869 (0.1 μg/μL), or GW4869 + FB-Exos (4 μg/μL) was injected subcutaneously around each wound (4 sites) at 0, 2, 4, and 6 days after injury. For diabetic mice, 50 μL of drug carrier (PBS) or FB-Exos (4 μg/μL) was injected locally at 2, 4, and 6 days after injury. The wound area was photographed with a digital camera at 2, 4, 6, and 8 days after wounding. The wound healing rate was calculated using an image software (NIH, USA) as follows: healing rate (%) = $(WA_i - WA_n)/WA_i \times 100\%$, where WA_i is the initial wound area and WA_n is the wound area on the *n*-th day after injury.

Downloaded from academic.oup.com/burnstrauma/article/doi/10.1093/burnst/tkae071/8151405 by guest on 13 October 2026

Immunostaining analysis

Immunofluorescence staining was conducted on formalin-fixed paraffin-embedded or cryosectioned wound tissues permeabilized with 0.5% Triton X-100 and immunolabeled overnight with specific antibodies against CD31 (1:200), VEGF-A (1:200), and VEGFR2 (1:200), followed by incubation with fluorescence-conjugated secondary antibodies (all from Abcam). Nuclei were counterstained with 1× DAPI solution. Images were acquired under a confocal microscope (Olympus). For immunohistochemical staining, the paraffin-embedded sections were dewaxed, antigenically repaired, blocked, and incubated with the primary antibody VEGF-A (Abcam).

Wound blood perfusion analysis

Wound angiogenesis was also assessed by a laser Doppler imaging system to evaluate microvascular blood flow in wound beds and peri-wound skin over time as described earlier. The mice were anesthetized and held immobile in a mold. Consecutive scans were acquired via the RFLSI III system over the indicated time intervals until day 8 post-wounding to quantify perfusion. Wound areas were identified by contouring scan images via an ROI tool to quantify average flow values. Contralateral intact skin served as control tissue for comparison at each time point for each mouse.

Enzyme-linked immunosorbent assay

Conditioned media supernatants from vECs were collected and analyzed using human VEGF-A enzyme-linked immunosorbent assay (ELISA) kits according to the manufacturer's instructions (R&D Systems). The curve was generated per standard protein OD values followed by evaluating the concentration of VEGF-A in conditioned media.

Real-time quantitative PCR

For cell and wound tissues, total RNA was extracted via TRIzol reagent (Thermo Fisher Scientific, USA) according to the manufacturer's protocol. The total cDNA was reverse transcribed from equal amounts of RNA (1 μg) using a reverse transcription kit (TOYOBO, Japan). mRNA expression was then quantified using SYBR Green PCR Master Mix according to primer sequences. These primer sequences used are as follows: HIF-1α (forward) GGTCTAGGAAACTCAA AACCTGA, (reverse) TGGCTGCATCTCGAGACTTT; VEG FA (forward) AAGGGGCAAAAACGAAAGCG, (reverse) CTCCAGGGCATTAGACAGCA; VHL (forward) ACGGAC AGCCTATTTTTGCCAA, (reverse) GTCCAGTCTCCTGTA ATTCTCA; VEGFR2 (forward) ATGCATCCTTGCAGGAC CAA, (reverse) TCTAGGACTGTGAGCTGCCT; GAPDH (forward) CAGGAGGCATTGCTGATGAT, (reverse) GAAG GCTGGGGCTCATTT. All primers were generated and provided by Sangon Biotech. The expression of all target mRNAs was normalized to that of GAPDH.

For microRNA analysis, total RNA enriched for small RNA was extracted from cells using miRNA kits (Sangon). cDNA was synthesized using a cDNA synthesis kit (Sangon) based on the stem-loop method, and target miR-24-3p was quantified via qRT-PCR via Taqman Fast Advanced master mix (Vazyme) and specific primers on a QuantStudio 6 Flex system (Bio-Rad). The expression of miRNA was normalized to that of U6 snRNA.

Co-immunoprecipitation

Co-immunoprecipitation kits (Beyotime) were used for experiments after total protein was extracted with cell lysis buffer. Briefly, the protein samples were incubated overnight at 4°C with magnetic beads combined with antibodies or normal IgG. After the protein sample was combined with the corresponding antibody, the suspension was eluted and separated by magnetic beads for further western blot experiments as described above. The following antibodies were used: anti-VHL (1:500, Santa Cruz, sc-135657), anti-HIF-1α (1:500, Santa Cruz, sc-17811), anti-PHD2(1:500, Santa Cruz, sc-271835), and anti-ubiquitin (1:500, Santa Cruz, sc-8017).

Western blot

Cells or tissues were lysed using 1× RIPA buffer supplemented with 1× protease/phosphatase inhibitors (Beyotime) followed by sonicating briefly. All protein concentrations were detected using a BCA kit (Thermo Fisher Scientific). Using a standard protocol, equal amounts of proteins with 1× loading buffer were resolved using 7.5%–12.5% gels (Epizyme) and transferred onto PVDF membranes (Merck) on ice. These membranes were blocked in 5% nonfat milk (Epizyme) and incubated overnight with specific primary antibodies (all antibodies are from Cell Signaling Technologies unless indicated otherwise): VEGFA (1:1000), VEGFR2 (1:1000), phospho-VEGFR2 (p-VEGFR2, 1:1000), HIF1-α (1:1000), PHD2 (1:1000), VHL (1:1000), β-actin (1:1000), AKT (1:1000), phospho-AKT (p-AKT, 1:1000), mTOR (1:1000), phospho-mTOR (p-mTOR, 1:1000), and GAPDH (1:1000). Corresponding HRP-conjugated secondary antibodies (Beyotime, 1:3000) were incubated for 1 h at room temperature before chemiluminescent detection under an iBright imaging system (Thermo Fisher Scientific).

Statistical analysis

Data represent means ± SD values combined from duplicate independent experiments unless otherwise stated. Data were analyzed using a GraphPad Prism 8.0 software, in which groups were compared by unpaired Student's *t*-test with Shapiro–Wilk normality for two groups and one-way or two-way ANOVA with Tukey's multiple comparisons for more than three groups. $P < .05$ was considered as statistically significant.

Results

Exosomes are essential paracrine effectors of fibroblast-stimulated angiogenesis *in vitro*

We first aimed to delineate stromal regulation of angiogenesis using an *in vitro* model where primary mouse dermal fibroblasts were co-cultured with vascular endothelial cells (vECs). Fibroblasts stimulated vECs tube-like structure formation on Matrigel in a dose-dependent manner (Figure 1a). To ascertain if this pro-angiogenic effect was contact dependent, we utilized transwell co-cultures with porous inserts preventing cell–cell contact. Intriguingly, separated co-cultures retained the ability of fibroblasts to enhance vECs tubulogenesis, indicating the involvement of a paracrine stimulus (Figure 1b).

Since exosomes represent a predominant means of paracrine communication through the intercellular transfer of bioactive proteins, lipids, and genetic material, we hypothesized a role for exosomes in fibroblast-mediated angiogenesis. To test this,

Downloaded from academic.oup.com/burnstrauma/article/doi/10.1093/burnst/tkae071/8151405 by guest on 13 October 2026

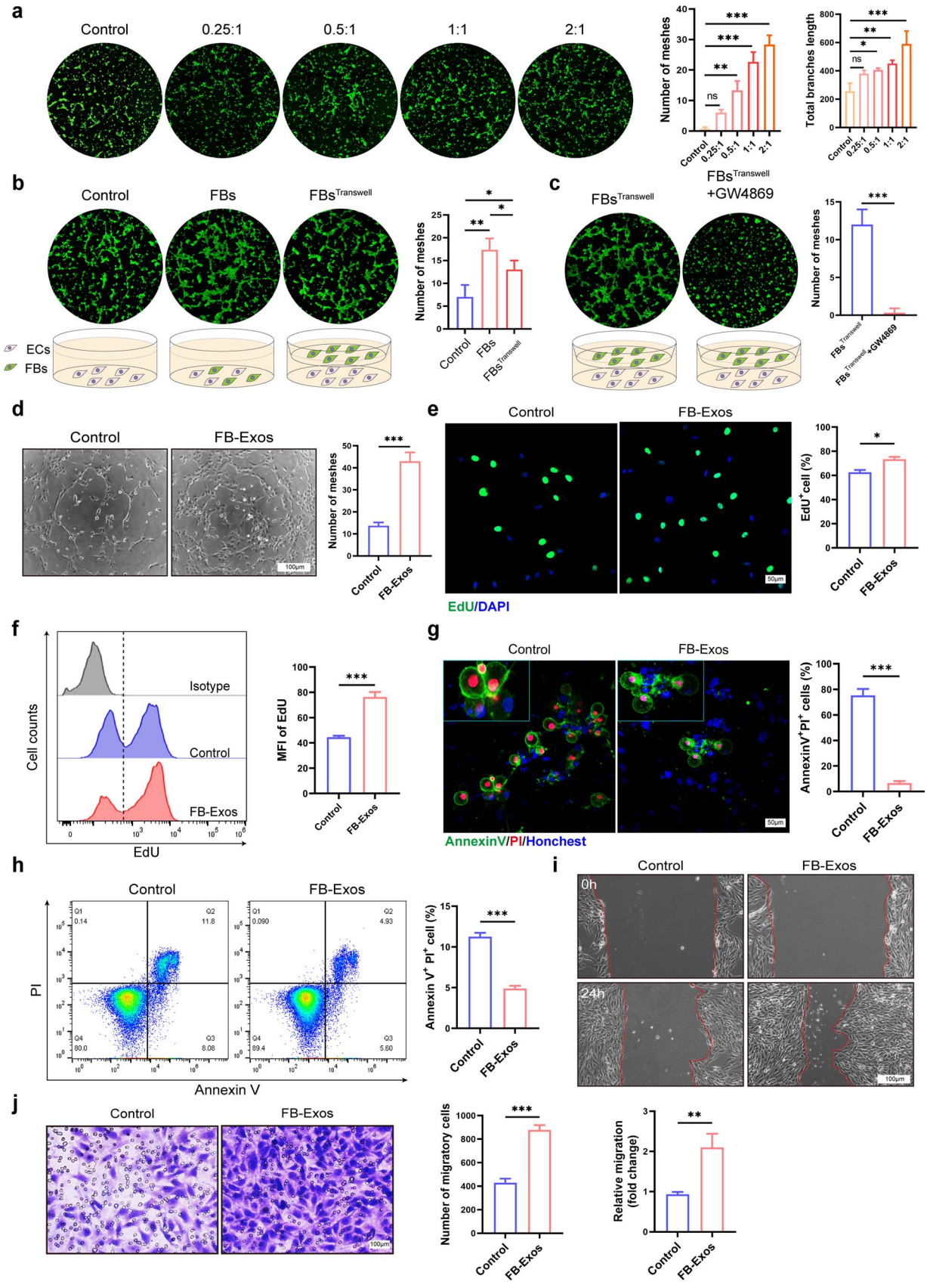

Figure 1. Fibroblasts enhance angiogenesis via paracrine transfer of exosomes in vitro. (**a**–**d**) Representative tube-like structures of vECs were visualized by confocal or light microscopy in the indicated groups. Bar: 100 μm. (**e**–**h**) The effects of FB-Exos on vEC (e, f) proliferation and (g, h) apoptosis were examined by immunofluorescence and flow cytometry. Bar: 50 μm. (**i**, **j**) The migration of vECs was detected by (i) scratch and (j) transwell assays. Bar: 100 μm. *P*-value was calculated by one-way ANOVA with Tukey's multiple comparisons (a, b) or unpaired *t*-test with Shapiro–Wilk normality test (c–j). $^{*}P < 0.05$; $^{**}P < 0.01$; $^{***}P < 0.001$. FBs fibroblasts; vECs, vessel endothelial cells

Downloaded from academic.oup.com/burnstrauma/article/doi/10.1093/burnst/tkae071/8151405 by guest on 13 October 2026

we pharmacologically inhibited exosome biogenesis using GW4869 reagents, a neutral sphingomyelinase inhibitor that blocks ceramide-triggered inward budding of multivesicular bodies (MVBs) to yield exosomes [33]. Strikingly, GW4869 treatment ablated the ability of fibroblasts to stimulate vECs tubule formation (Figure 1c). This strongly implicated exosomes as the primary paracrine pro-angiogenic stimuli elaborated by fibroblasts.

To ascertain whether fibroblast-derived exosomes (FB-Exos) exert direct pro-angiogenic effects, FB-Exos were fluorescently labeled and applied to vEC cultures. Rapid endocytosis and cytoplasmic localization of labeled exosomes were visualized in vECs within 6 h, confirming efficient cellular uptake (Supplementary Figure 1g). Functionally, FB-Exos strongly promoted tubule formation by vECs seeded on Matrigel, with >3-fold increases in number of meshes quantified (Figure 1d).

During new blood vessel growth, proliferation, directed migration, and survival of sprouting endothelial tip cells represent essential processes coordinated by pro-angiogenic signals. We discovered that FB-Exos increased the fraction of S-phase replicating vECs by 13%, as determined by EdU pulsing experiments (Figure 1e, f). FB-Exos also exhibited pro-survival effects, rescuing serum-deprived apoptotic vECs from cell death. Annexin-V staining quantified a ~60% reduction in apoptosis upon FB-Exos treatment (Figure 1g, h). Scratch wound migration assays showed ~2.2-fold faster closure of cell-free areas over 24 h with FB-Exos stimulation (Figure 1i). Analogous increases in invading cell numbers (~2-fold) were obtained by invasion assays, substantiating enhanced endothelial cell motility (Figure 1j).

These results demonstrate that FB-Exos stimulates multiple facets of angiogenesis *in vitro*, including proliferation, survival, migration, and tubulogenesis. Exosome release appears vital for fibroblast-mediated regulation of endothelial behavior.

Fibroblast exosomes are indispensable for cutaneous wound angiogenesis and healing

Having delineated the pro-angiogenic properties of FB-Exos *in vitro*, we interrogated their functional relevance *in vivo* using a murine wound healing model. Full-thickness 6-mm dorsal skin punch biopsy wounds were generated in WT mice. Following injury, wounds were injected subcutaneously with either the GW4869 or vehicle control at days 0, 2, 4, and 6. Strikingly, inhibition of endogenous exosome production markedly impeded wound closure dynamics macroscopically (Figure 2a), with reduced re-epithelialization and granulation tissue formation quantified histologically (Supplementary Figure 2a).

To ascribe this wound healing defect specifically to loss of fibroblast exosome production, exogenously isolated FB-Exos were topically applied onto GW4869-treated wounds at days 0, 2, 4, and 6. Administration of supplemental FB-Exos largely restored normal healing progression, including wound closure rates (Figure 2a), re-epithelialization, and the formation of granulation tissues (Supplementary Figure 2a). This rescue experiment confirms that fibroblast-derived exosomes are indispensable paracrine effectors regulating cutaneous wound repair.

Functionally, we examined if the macroscopic wound healing delay observed upon GW4869 treatment and loss of endogenous exosomes was underpinned by angiogenesis inhibition. H&E staining (Supplementary Figure 2b) and CD31 immunofluorescence (Figure 2b) verified markedly reduced microvessel density and endothelial cell infiltration within granulation tissues of GW4869-treated wounds at days 2 and 4 post-injury. *In vivo* vascular perfusion analyses using a laser Doppler further substantiated angiogenesis defects, with significantly lowered wound site blood flow in the absence of endogenous exosomes at day 3 (Figure 2c). Peak levels of revascularization were also delayed, occurring at day 6 rather than day 4 post-wounding in GW4869-treated group. Remarkably, topical administration of FB-Exos onto GW4869-treated wounds corrected the aberrant neovascularization, restoring normal endothelial cell infiltration, vessel density, and tissue perfusion (Figure 2b, c).

These striking *in vivo* results establish fibroblast-secreted exosomes as indispensable paracrine stimuli that coordinately regulate angiogenesis to enable efficient cutaneous wound repair.

FB-Exos activates VEGF–VEGFR2 signaling by increasing ligand and receptor levels

The VEGF–VEGFR2 signaling axis represents the archetypal pathway governing developmental and pathological angiogenesis [34]. We discovered that FB-Exos strongly stimulated both intracellular VEGF-A protein accumulation (Figure 3a, b, and d) and secreted VEGF-A levels (Figure 3c) in vEC cultures, with higher concentrations detected by ELISA. This was accompanied by 6-fold increases in VEGFA mRNA expression (Figure 3f), indicating that FB-Exos elicits VEGF production at multiple levels. Furthermore, immunofluorescence staining results corroborated greater cytoplasmic VEGF-A localization and expression following FB-Exos treatment (Figure 3b).

VEGFA signals principally through VEGFR2 displayed on endothelial cells, stimulating receptor dimerization and auto/paracrine propagation of downstream signaling cascades regulating proliferation and migration [35]. We discovered that FB-Exos enhanced VEGFR2 transcript levels by ~10-fold in vECs (Figure 3g). Cell surface VEGFR2 protein was also elevated ~1.4-fold (by flow cytometry) (Figure 3e). Total VEGFR2 protein increases were affirmed by immunoblotting and immunofluorescence (Figure 3h, i). Furthermore, the phosphorylation of VEGFR2 at tyrosine residues was intensely stimulated by FB-Exos, indicative of receptor activation (Figure 3h, i). Besides the activation of VEGFR2, we also found that AKT–mTOR signaling pathway related to angiogenesis was significantly activated by FB-Exos in a time-dependent manner (Supplementary Figure 3a).

In vivo, the inhibition of fibroblast exosome production in dorsal wounds via GW4869 injection markedly suppressed wound site immunopositivity for both VEGFA and VEGFR2, with fewer number of positive cells and lower fluorescence intensity (Figure 3j, Supplementary Figure 3b). As previously, topical administration of FB-Exos onto these wounds strikingly rescued both VEGFA and VEGFR2 expression.

Hence, our results demonstrate that fibroblast-secreted exosomes potently activate the master VEGF–VEGFR2 angiogenic signaling axis by increasing ligand and receptor levels in target endothelial cells.

FB-Exos enhances HIF-1α stability by downregulating VHL E3 ubiquitin ligase

To identify upstream regulators of FB-Exos-induced VEGF–VEGFR2 signaling, we analyzed the central transcriptional

Downloaded from academic.oup.com/burnstrauma/article/doi/10.1093/burnst/tkae071/8151405 by guest on 13 October 2026

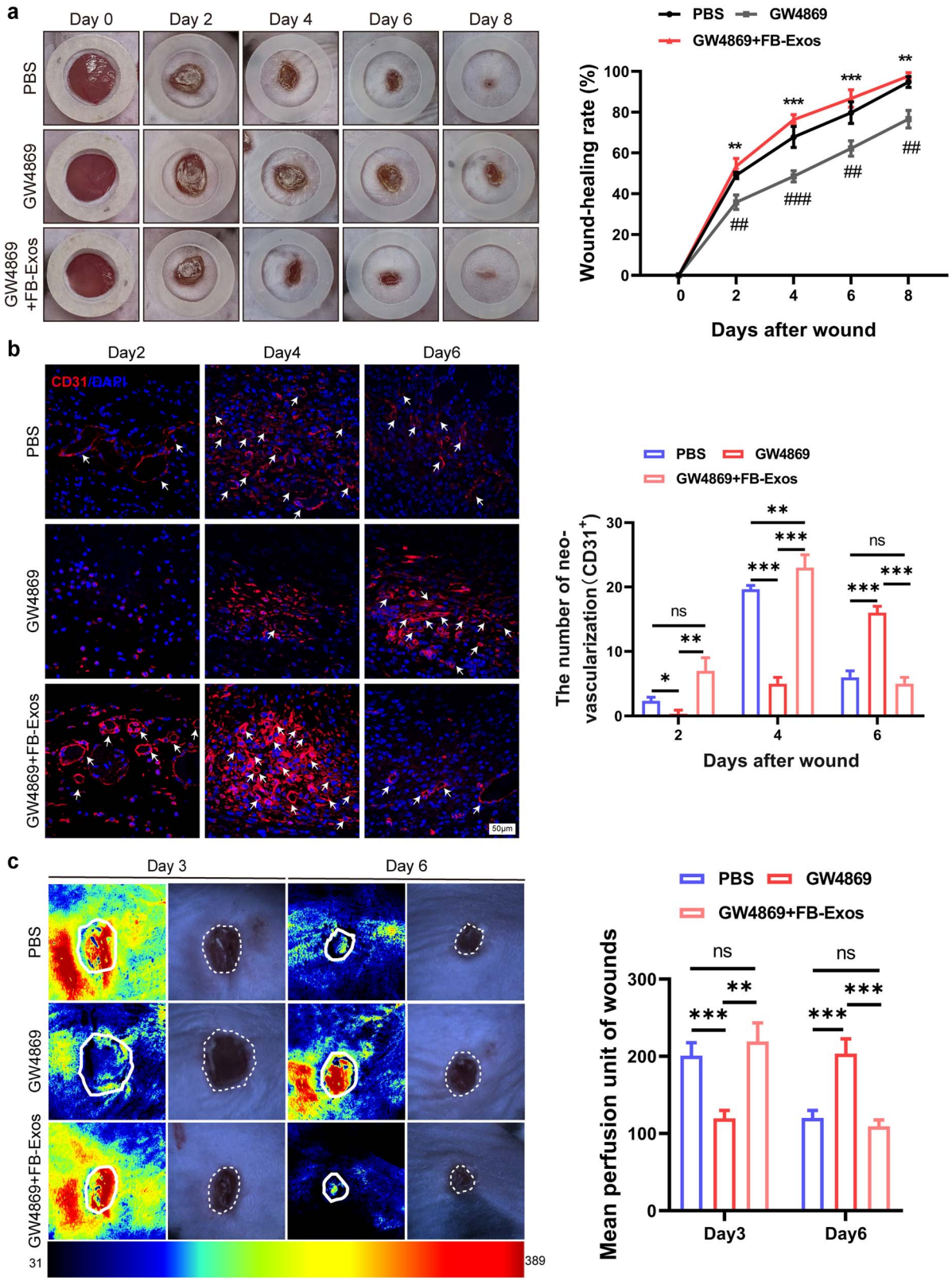

Figure 2. FB-Exos play irreplaceable roles for angiogenesis and wound healing *in vivo*. (**a**) Wound closure was analyzed in mice injected subcutaneously with PBS, GW4869, or GW4869 + FB-Exos immediately after wounding. *Means GW4869 vs. GW4869 + FB-Exos; #means PBS vs. GW4869 ($n = 6$ mice per group). (**b**) The positive CD31 area in wound tissue was measured by immunofluorescence staining (the white arrows represent CD31-positive neovascular). Bar: 50 μm ($n = 6$ mice per group). (**c**) The blood flow status of the wound area was monitored by a laser Doppler monitor ($n = 6$ mice per group). *P*-value was calculated by two-way ANOVA with Tukey's multiple comparisons. $^{*}P < .050.05$; $^{**}P < 0.01$; $^{***}P < 0.001$. *PBS*, phosphate buffer solution

Downloaded from academic.oup.com/burnstrauma/article/doi/10.1093/burnst/tkae071/8151405 by guest on 13 October 2026

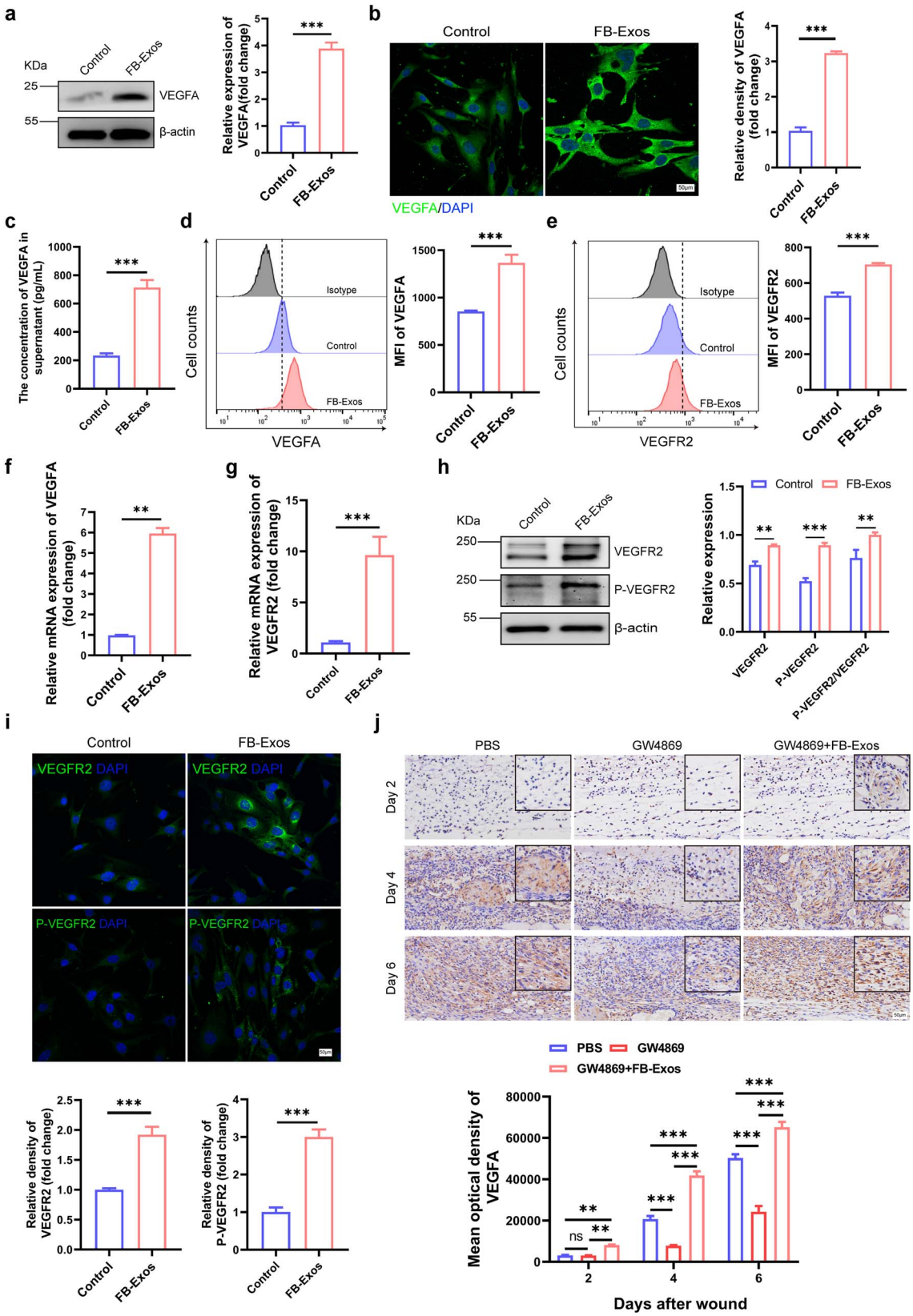

Figure 3. FB-Exos activate VEGF–VEGFR2 pro-angiogenic signaling in endothelial cells. (**a**–**d**) The expression levels of VEGFA were evaluated by (a) immunoblotting, (b) immunofluorescence, (c) ELISA, and (d) flow cytometry ($n = 3$ per group). Bar: 50 μm. (**e**) Representative histograms for VEGFR2 ($n = 3$ per group). (**f**, **g**) Quantitative expression graphs of (f) VEGFA and (g) VEGFR2 mRNA ($n = 5$ per group). (**h**, **i**) Representative (h) immunoblotting and (i) immunofluorescence images for VEGFR2 and P-VEGFR2. Bar: 50 μm ($n = 3$ per group). (**j**) Representative immunohistochemical images for VEGFA in granulation tissues. Bar: 50 μm ($n = 6$ mice per group). *P*-value was calculated by unpaired *t*-test with Shapiro–Wilk normality test (a–i) or two-way ANOVA with Tukey's multiple comparisons (j). $^{*}P < 0.05$; $^{**}P < 0.01$; $^{***}P < 0.001$. *VEGFA* vascular endothelial growth factor A, *VEGFR2* vascular endothelial growth factor receptor 2

Downloaded from academic.oup.com/burnstrauma/article/doi/10.1093/burnst/tkae071/8151405 by guest on 13 October 2026

mediator hypoxia-inducible factor-1 alpha (HIF-1α). While HIF-1α mRNA levels were unchanged (Supplementary Figure 4a), FB-Exos treatment elicited ~2-fold increases in HIF-1α protein with heightened nuclear localization in vECs (Figure 4a, b). Analogously *in vivo*, immunofluorescence staining of wound granulation tissues showed GW4869-treated wounds harboring fewer HIF-1α-positive cells (~8%) than vehicle control wounds (~41%) at day 2. Topical application of FB-Exos increased the fraction of HIF-1α+ cells to ~48% at day 2 (Figure 4c).

Cycloheximide chase experiments investigated whether FB-Exos regulated HIF-1α stability to block new protein translation and assess degradation kinetics. We discovered delayed HIF-1α turnover upon FB-Exos stimulation, increasing estimated protein half-life from ~60 to >90 min and substantially prolonging detection (Figure 4d). In tandem, HIF-1α ubiquitin-tagging was reduced following FB-Exos treatment (Figure 4e; Supplementary Figure 4b). Although oxygen-sensor PHD2 levels were slightly lowered, FB-Exos strongly suppressed both transcript and protein of the critical VHL E3 ubiquitin ligase that mediates proteasomal degradation of hydroxylated HIF-1α (Figure 4f; Supplementary Figure 4c, d). Immunoprecipitation assays demonstrated that FB-Exos disrupted VHL binding to HIF-1α without affecting PHD2 interactions (Supplementary Figure 4e). This explains enhanced HIF-1α stability due to reduced proteasomal degradation.

FB-Exos elicits HIF-1α protein stabilization by selectively downregulating its key negative regulator VHL ubiquitin ligase. This augments HIF-1α-dependent transcriptional activation of the VEGF–VEGFR2 signaling axis.

miR-24-3p regulates VHL suppression to modulate HIF-1α stability in endothelial cells stimulated by fibroblast-derived exosomes

We investigated the identity and functional relevance of specific components in fibroblast-derived exosomes (FB-Exos) regulating VHL levels and HIF-1α stability in recipient cells. Small RNA sequencing identified 17 miRNAs predicted to target proteins in the ubiquitin-mediated proteolysis pathway. Using TargetScan analyses, miR-24-3p and miR-541-5p were predicted to directly inhibit VHL. Pathway annotation confirmed the established roles of miR-24-3p in regulating ubiquitination and cell signaling cascades (Supplementary Figure 5a, b).

Among candidate miRNAs, qPCR analysis verified that miR-24-3p was highly enriched in FB-Exos, being ~35-fold more abundant than miR-541-5p (Supplementary Figure 5c). Correspondingly, incubation of vECs with FB-Exos elevated intracellular miR-24-3p levels ~3-fold, substantiating efficient exosomal transfer (Figure 5a).

To conclusively evaluate miR-24-3p functionality, we generated fibroblasts overexpressing or suppressing miR-24-3p to establish exosomes enriched (~8-fold higher) or deficient (by ~65% knockdown) in miR-24-3p levels compared to control FB-Exos (Supplementary Figure 6a). Exosomes overexpressing miR-24-3p strongly reduced VHL protein levels by ~60% in recipient vECs, consequently increasing HIF-1α protein accumulation (Figure 5b, c) and VEGFA mRNA and protein expression (Supplementary Figure 6b, c). Significant suppression of VHL mRNA (~70% lower), but not HIF-1α mRNA, was also achieved (Supplementary Figure 6d). Reciprocal trends of VHL upregulation and HIF-1α destabilization were observed upon delivery of miR-24-3p-deficient exosomes to vECs (Figure 5b, c; Supplementary Figure 6b–d).

Functionally, heightened miR-24-3p cargo enhanced the ability of FB-Exos to stimulate tube-like structure formation of vECs (~1.6-fold increase in the number of meshes) (Figure 5d), proliferation (~30% higher) (Figure 5e), migration (~15% faster closure) (Supplementary Figure 6e), and anti-apoptosis (~2-fold lower apoptosis ratio) (Figure 5f). These angiogenesis-related bioactivities were partially countered by exosomes lacking miR-24-3p (Figure 5d–f; Supplementary Figure 6e). Delivery of miR-24-3p-rich exosomes mechanistically suppressed HIF-1α ubiquitination and proteasomal degradation in recipient vECs (Figure 5g). To verify whether VHL serves as the target of miR-24-3p, a dual-luciferase reporter assay was performed, and the results showed that the luciferase activity of mmu-miR-24-3p mimics has no significant difference compared to mimics NC group for both WT and MUT 293T cells (Supplementary Figure 6f), suggesting that miR-24-3p does not directly regulate the expression of VHL.

Collectively, our results reveal a vital role for FB-Exos-delivered miR-24-3p in suppressing endothelial VHL to modulate HIF-1α stabilization and consequent VEGF-dependent angiogenesis.

Topical FB-Exos administration rescues deficient wound neovascularization in type I diabetes

As a proof-of-concept for clinical translation, we evaluated if FB-Exos could rescue insufficient angiogenesis in a streptozotocin-induced mouse model of type I diabetes exhibiting characteristic microvascular deficits and delayed wound closure. Fluorescently labeled FB-Exos localized around keratinocytes and dermal vasculature when topically administered onto wounds and imaged at day 6, confirming sustained retention (Supplementary Figure 7a).

Using this classical animal model, we observed profound healing defects macroscopically and histologically within 8 days, including slower wound closure and reduced re-epithelialization (Figure 6a; Supplementary Figure 7b). Aberrant angiogenesis was substantiated by lowered microvessel density, attenuated endothelial cell infiltration, reduced wound site perfusion, and decreased expression of VEGFA (Figure 6b, c; Supplementary Figure 7c).

We observed that topical application of FB-Exos onto these chronic diabetic wounds strikingly ameliorated healing rate in a dose-dependent manner (Supplementary Figure 8a). To evaluate the potential impacts of different injury sizes on wound healing, the 8-mm- and 10-mm-diameter full-thickness diabetic wounds were created on dorsal skin of mice. As shown in Supplementary Figure 8B and C, the results showed that FB-Exos significantly promoted diabetic wound closure for both 8-mm- and 10-mm-diameter wounds. Therefore, these data indicate that FB-Exos play contributive roles for different-size diabetic wound repair. Macroscopic closure kinetics and re-epithelialization were improved significantly with FB-Exos treatment within 8 days (Figure 6a; Supplementary Figure 7b). Functionally, defective vascularization was rescued, with heightened endothelial cell recruitment, microvessel density, local blood flow quantified, and the expression of VEGFA (Figure 6b, c; Supplementary Figure 7c).

Downloaded from academic.oup.com/burnstrauma/article/doi/10.1093/burnst/tkae071/8151405 by guest on 13 October 2026

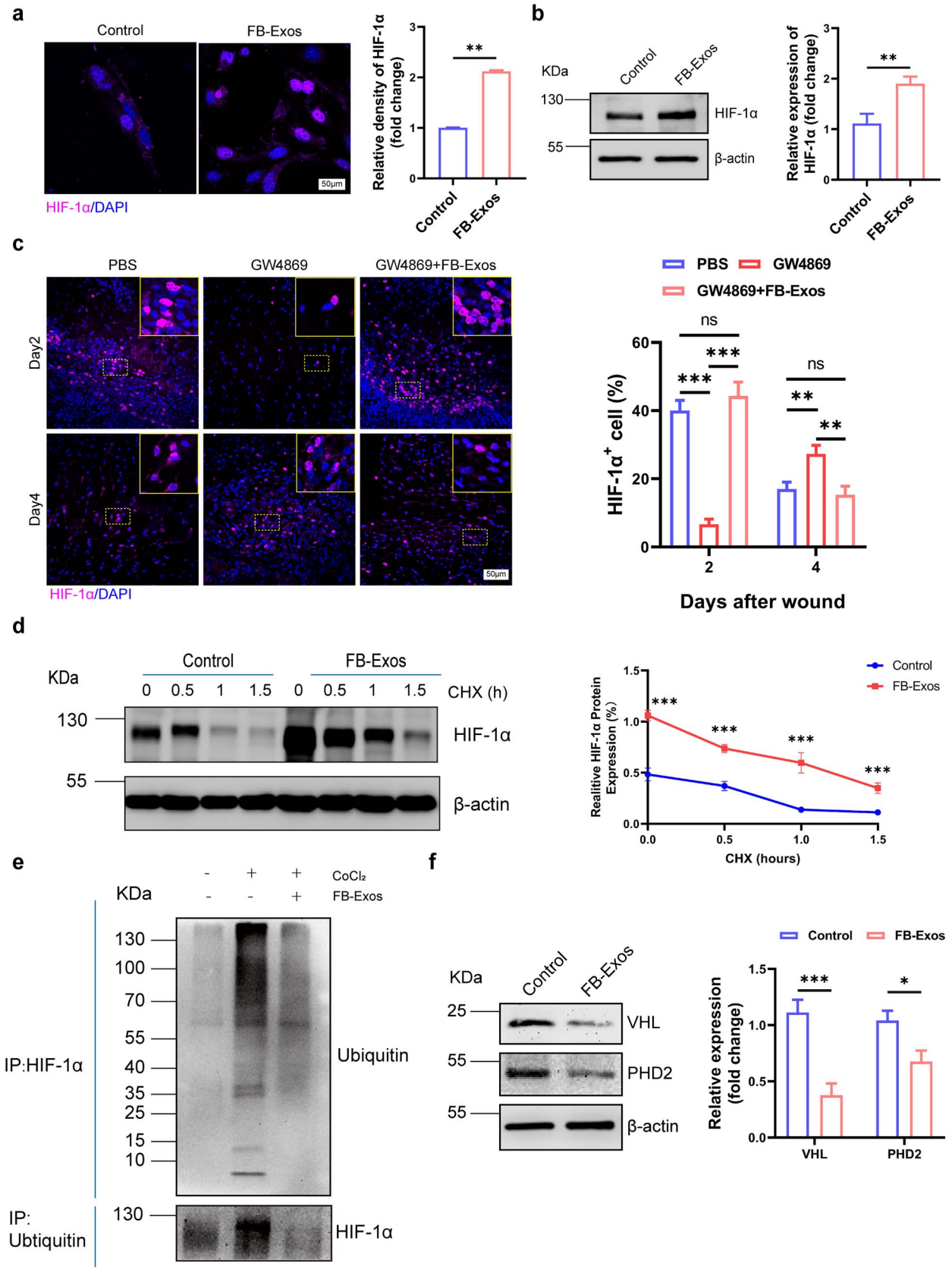

Figure 4. FB-Exos enhance HIF-1α stability by downregulating VHL in endothelial cells. (**a**, **b**) Representative (a) immunofluorescence and (b) immunoblotting images for HIF-1α. Bar: 50 μm ($n = 3$ per group). (**c**) Representative immunofluorescence images for HIF-1α in indicated group. Bar: 50 μm ($n = 6$ mice per group). (**d**) The expression of HIF-1α in vECs co-cultured with or without FB-Exos was detected ($n = 3$ per group). (**e**) Representative immunoblotting images for ubiquitin and HIF-1α in indicated groups ($n = 3$ per group). (**f**) Representative immunoblotting images for VHL and PDH2 ($n = 3$ per group). *P*-value was calculated by unpaired *t*-test with Shapiro–Wilk normality test (a, b, f) or two-way ANOVA with Tukey's multiple comparisons (c, d). $^{*}P < 0.05$; $^{**}P < 0.01$; $^{***}P < 0.001$. *HIF-1α* hypoxia-inducible factor 1 alpha, *VHL* von Hippel–Lindau, *PDH2* proline hydroxylases 2

Downloaded from academic.oup.com/burnstrauma/article/doi/10.1093/burnst/tkae071/8151405 by guest on 13 October 2026

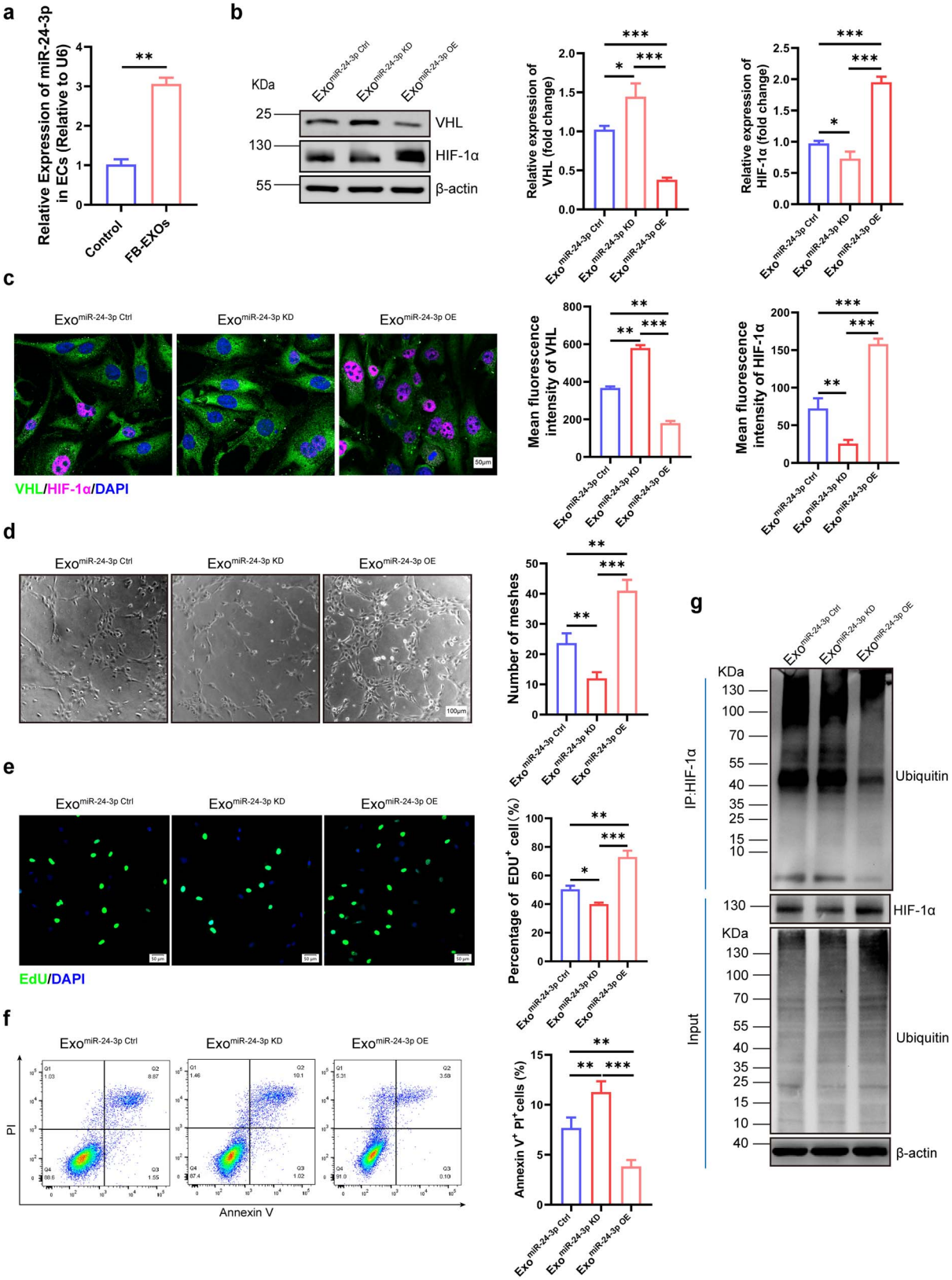

Figure 5. FB-Exos downregulated the expression of VHL by transferring miRNA-24-3p to vECs. (**a**) The expression level of miRNA-24-3p was examined by qRT-PCR ($n = 5$ per group). (**b**, **c**) Representative (b) immunoblotting and (c) immunofluorescence images for VHL and HIF-1α. Bar: 50 μm ($n = 3$ per group). (**d**) Representative tube-like structure images in indicated groups. Bar: 100 μm ($n = 3$ per group). (**e**) Representative immunofluorescence images for EdU. Bar: 50 μm ($n = 3$ per group). (**f**) Representative scatter diagram for Annexin-V and PI staining ($n = 3$ per group). (**g**) Representative immunoblotting images for ubiquitin and HIF-1α in indicated groups ($n = 3$ per group). *P*-value was calculated by unpaired *t*-test with Shapiro–Wilk normality test (a) or one-way ANOVA with Tukey's multiple comparisons (b–f). $^{*}P < 0.05$; $^{**}P < 0.01$; $^{***}P < 0.001$. *HIF-1α* hypoxia-inducible factor 1 alpha, *VHL* von Hippel–Lindau, *PDH2* proline hydroxylases 2

Downloaded from academic.oup.com/burnstrauma/article/doi/10.1093/burnst/tkae071/8151405 by guest on 13 October 2026

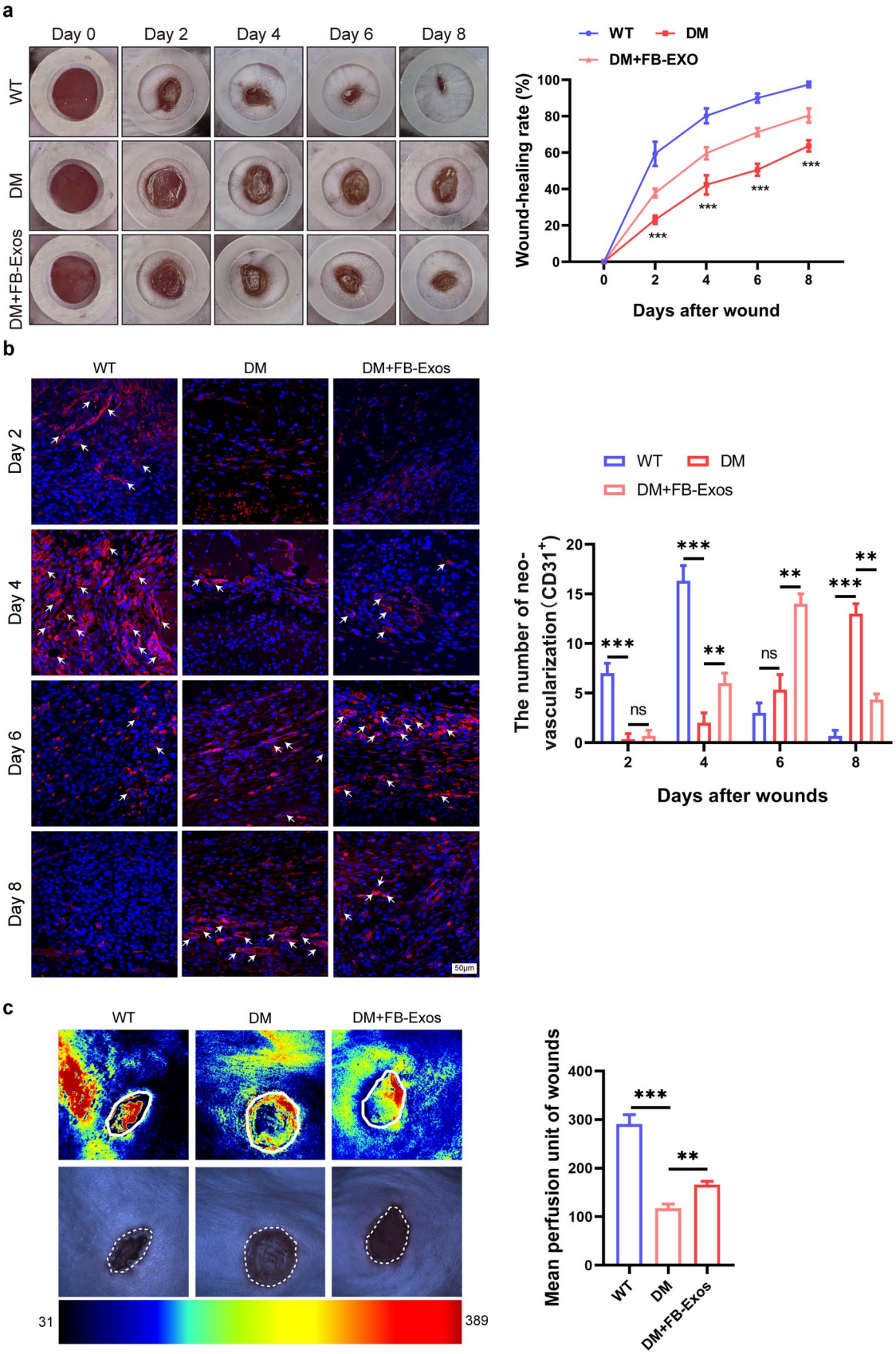

Figure 6. Fibroblast exosomes rescue insufficient neovascularization in diabetic wounds. (**a**) Representative images of wound size at different time points and wound healing curve ($n = 6$ mice per group). (**b**) The number of neovascularization ($CD31^+$) in wound granulation tissue was shown by immunofluorescence staining (the white arrows represent CD31-positive neovascular). Bar: 50 μm ($n = 6$ mice per group). (**c**) The blood flow status of the wound area was monitored by laser Doppler monitor ($n = 6$ mice per group). *P*-value was calculated by two-way ANOVA with Tukey's multiple comparisons (a, b) and one-way ANOVA with Tukey's multiple comparisons (c). $^*P < 0.05$; $^{**}P < 0.01$; $^{***}P < 0.001$

Downloaded from academic.oup.com/burnstrauma/article/doi/10.1093/burnst/tkae071/8151405 by guest on 13 October 2026

Hence, FB-Exos administration potently activates angiogenesis to improve wound healing dynamics in diabetes. Our results provide a compelling rationale for the translational development of acellular FB-Exo therapies to treat vascular insufficiency and chronic wounds.

Discussion

Complex heterocellular communication enables physiological angiogenesis during tissue repair [1,5,8]. In addition to facilitating canonical VEGF–VEGFR2 signaling, endothelial tip cells integrate inputs from diverse parenchymal, mural, and immune cells to coordinate sprouting [9,10]. In response, the activated endothelium secretes perivascular niche factors that promote cellular recruitment and ECM production [1]. However, the mechanistic delineation of pathways facilitating such intricate multicellular crosstalk has remained challenging *in vivo*. Our findings reveal a vital role for fibroblast-secreted exosomes as essential paracrine mediators that activate angiogenesis during cutaneous wound healing. We demonstrate that FB-Exos potently stimulates VEGF-dependent signaling, proliferation, migration, and tubulogenesis in endothelial cells. Sustained inhibition of endogenous exosome production markedly suppressed neovascularization, delaying wound closure. The topical provision of exogenous FB-Exos reversed these defects. We further established miR-24-3p as a key genetic cargo delivered by FB-Exos that enhances HIF-1α stability by downregulating VHL ubiquitin ligases in the recipient endothelium. The administration of FB-Exos potently stimulated revascularization in a diabetic wound healing model, underscoring their translational potential.

Reciprocal crosstalk between dermal fibroblasts and microvascular endothelial cells represents an archetypal example of heterocellular communication that governs physiological and pathological angiogenesis [5,8]. Genetic murine models in which dermal fibroblasts are selectively ablated during cutaneous development or wound repair substantiate their indispensable roles in coordinating epithelial and endothelial behavior [8]. Fibroblasts have been proposed to regulate the "angiogenic switch"; however, the underlying mechanisms beyond soluble VEGF secretion remain undefined [12,24]. Our results directly demonstrate the essential functionality of fibroblast-derived exosomes as predominant paracrine effectors that stimulate angiogenesis during tissue repair. The pharmacological inhibition of exosome genesis effectively suppressed endothelial activation and neovascularization despite maintaining intercellular contact or transmitting soluble mediators across transwells. The topical provision of supplemental human fibroblast exosomes completely corrected these defects. To our knowledge, this represents the first direct genetic evidence substantiating the indispensable roles of parenchymal cell–derived exosomes in physiological angiogenesis *in vivo*. We propose that, under homeostatic conditions, tissue-specific exosomes serve as key endogenous mediators facilitating context-dependent intercellular communication. Further investigation of this model in diverse regenerative settings would be illuminating.

We systematically delineated downstream signaling events using reductionist *in vitro* systems to understand how fibroblast exosomes elicit such profound endothelial activation. FB-Exos strongly stimulate VEGF–VEGFR2 signaling by concomitantly increasing both ligand and receptor levels effectively establishing a positive feed-forward loop that amplifies pathway flux. Consequently, endothelial proliferation, migration, and tubulogenesis are all enhanced. Selective inhibition of the VEGF–VEGFR2 axis could clarify whether alternative pathways contribute to FB-Exos bioactivity. Nevertheless, our findings align with previous findings on endothelial exosomes, which similarly activate VEGF autoregulatory loops in the target endothelium [17]. Upstream of VEGF, we discovered the selective stabilization of the master transcriptional regulator HIF-1α. By suppressing PHD-VHL-mediated ubiquitination and degradation, FB-Exos enhanced HIF-1α nuclear retention to activate target genes such as VEGFA. These results illuminate a cogent mechanistic cascade centered on HIF–VEGF pathway activation underlying exosome bioactivity. It would be interesting to evaluate whether FB-Exos also modulates other angiogenesis-regulating genes. The effects may also be endothelial cell subtype specific, with microvascular endothelial cells from the skin and cardiac tissue exhibiting distinct HIF-1α responsiveness [36].

A key objective has been identifying specific exosome components that modulate signaling in recipient cells [13,18]. We identified miR-24-3p as a vital genetic cargo delivered by FB-Exos that regulates HIF–VEGF pathway activity using an unbiased sequencing approach coupled with functional validation. By inhibiting the expression of VHL mRNA, exosomal miR-24-3p inhibited VHL translation, explaining the enhanced HIF-1α protein stability. miR-24-3p joins exosome-transferred angiomiRs such as miR-126 and miR-296, which stimulate ischemia-mediated revascularization by suppressing negative regulators of VEGF signaling such as SPRED1 and PHD2 [37–39]. Our results extend this paradigm, revealing that miR-24-3p is an additional exosomal angiomiR that targets the key E3 ubiquitin ligase VHL. It would be interesting to conduct epistasis experiments in which miR-24-3p was inhibited in the context of endogenous FB-Exos to evaluate the functional importance of exosomal proteins, mRNAs, and miRNAs. The selective loading of miR-24-3p into FB-Exos, rather than its retention in fibroblasts that highly endogenously express this miRNA, implies the presence of active packaging mechanisms. RNA-binding proteins may recognize miR-24-3p to enable its encapsulation into MVBs. In addition to miR-24-3p, we also found that multiple miRNAs in FB-Exos were related to angiogenesis by performing GO and KEGG pathway analyses associated with angiogenesis via high-throughput miRNA sequences (Supplementary Figure 5d, e). Elucidating miRNA packaging mechanisms might explain how angiogenic potential is asymmetrically partitioned into secreted exosomes rather than retained by activated fibroblasts. From a therapeutic standpoint, understanding loading mechanisms would enable the engineering of artificial exosomes stably enriched with pro-angiogenic miRNAs.

Chronic diabetic wounds exhibit paradoxical VEGF overexpression yet insufficient angiogenesis, undermining tissue repair [9,10]. Using a murine diabetic wound healing model, we discovered that the topical administration of human FB-Exos could correct neovascularization deficits. This finding validates the functionality of our reductionist *ex vivo* observations in a complex *in vivo* pathological setting. Intriguingly, a xenogeneic source of exosomes appeared active, implying the conserved bioactivity of angiogenic stimuli across species lines. It would be relevant to test the efficacy of

Downloaded from academic.oup.com/burnstrauma/article/doi/10.1093/burnst/tkae071/8151405 by guest on 13 October 2026

autologous fibroblast-derived exosomes harvested from diabetic patients, to evaluate their comparative potency [40]. This would provide greater preclinical validation before initiating clinical trials. Testing additional models of chronic wounds arising from venous stasis, vasculopathy, or irradiation in parallel would allow for broader applicability [10,41]. Comparing the relative functionality of fibroblasts with that of endothelial cell–derived exosomes in rescuing vascularization defects would also be informative [12,17,40]. In terms of therapeutic safety, exosomes appear to be well tolerated without observable adverse effects in our study or in previous reports in which high systemic doses were administered across species [40,42]. Because they are derived from syngeneic or autologous sources, compared with allogeneic cell therapy, exosomes are also expected to be minimally immunogenic [11,43,44]. However, formal toxicity analyses with long-term administration over months would provide reassurance before patient trials.

Our results carry salient implications on several fronts. First, we establish a vital functional role for tissue parenchymal cell–derived exosomes as physiological mediators of paracrine signaling that can be harnessed therapeutically. Second, we provide an example of integrated biological systems analysis bridging exosomal cargo identification with functional validation to demonstrate target gene modulation underlying angiogenesis stimulation. Third, we develop key principles underlying mechanism-based therapeutics centered on specific exosome-mediated transfer of pro-angiogenic miR-24-3p. Our findings provide a compelling rationale for developing acellular biologics using fibroblast-derived exosomes to treat vascular deficiency underlying chronic wound pathology. The striking rescue of deficient neovascularization via simple topical administration establishes a proof-of-concept for the therapeutic efficacy of FB-Exos. Because they are acellular, FB-Exos can overcome the scalability, manufacturing, storage, transport, and regulatory hurdles facing cell therapies [32,45]. They also circumvent the bioavailability limitations of recombinant angiogenic proteins with short half-lives, which require frequent application [10]. Furthermore, harnessing endogenous vesicles leverages physiological mechanisms of intercellular communication for tissue repair [16,46]. Our approach represents a template for developing extracellular vesicle therapeutics by revealing the mechanistic links between exosomal cargo and functionality. Systematically evaluating secretion from diverse cellular sources would provide candidate vesicles for regenerative applications beyond angiogenesis, encompassing dermal, neural, osseous, and muscular tissue repair [45,47–49]. Profiling cargo signatures would provide an understanding of how parent cell physiology governs exosome bioactivity [46]. Identifying enriched biologically active components that confer target cell specificity would rationalize manufacturing design [50]. Engineering artificial exosomes by overexpressing specific miRNAs or knocking down of deleterious transcripts may optimize therapeutic potency [40,51]. Our finding that miR-24-3p levels are rate limiting, with overexpression enhancing FB-Exo bioactivity, substantiates this approach. Furthermore, editing membrane proteins to append tissue-specific targeting peptides or circulating half-life extension domains may improve their localization and retention upon systemic administration [40,52,53]. Integrating such biological insights to customize and control exosome content and biodistribution would enable the next generation of engineered extracellular vesicular therapies.

Our findings demonstrated that fibroblast-derived exosomal miR-24-3p accelerates cutaneous wound healing in WT mice by promoting angiogenesis appear to contradict the results reported by Xu *et al*. [54]. In their study, inhibition of miR-24-3p expression enhanced angiogenesis and wound repair in WT mice by targeting PIK3R3. This discrepancy in outcomes highlights the complex and context-dependent functions of miR-24-3p in regulating angiogenesis. One potential explanation for this contradiction lies in the different experimental approaches used. We specifically investigated the effects of fibroblast-exosomal miR-24-3p delivery, while Xu *et al*. modulated global cellular miR-24-3p levels. The exosomal packaging and targeted delivery of miR-24-3p may elicit distinct functional outcomes compared to broader systemic effects. Additionally, the molecular targets and signaling pathways regulated by miR-24-3p may differ depending on the cellular context. While our study identified VHL as a critical target mediating the pro-angiogenic effects of miR-24-3p, Xu *et al*. demonstrated that PIK3R3 is a key target responsible for the anti-angiogenic effects of miR-24-3p. These findings suggest that miR-24-3p may regulate different downstream effectors and pathways, leading to opposing outcomes in angiogenesis regulation. It is important to note that miRNAs can exert pleiotropic effects by targeting multiple mRNAs, and their functions may be context dependent, varying across different cell types, physiological conditions, and disease states. Further studies are needed to elucidate the mechanisms underlying these contradictory observations and to delineate the specific conditions under which miR-24-3p exerts pro- or anti-angiogenic effects.

Conclusions

In conclusion, our findings elucidate fibroblast-derived exosomes as critical regulators that activate angiogenesis programs during tissue repair. We establish central roles for exosomal miR-24-3p in stimulating endothelial HIF-VEGF signaling by inhibiting VHL-mediated degradation. The clinical efficacy of FB-Exo administration in rescuing neovascularization deficits in diabetic wounds highlights promising translational potential. Further biological interrogation coupled with bioengineering innovation centered on harnessing secreted extracellular vesicles would propel the development of novel acellular biologics for regenerative medicine.

Acknowledgements

We thank all members of WFH and GXL laboratories for valuable discussion. The authors would like to thank the full support of the core facilities at the Institute of Burn Research, Southwest Hospital, Third Military Medical University. We thank GL, HMS, and JH providing discussion and suggestions for this manuscript.

Author contributions

Yunxia Chen (Investigation [Lead], Methodology [Lead]), Wenjing Yin (Investigation [Supporting]), Zhihui Liu (Investigation [Supporting]), Guang Lu (Investigation [Supporting]), Xiaorong Zhang (Investigation [Supporting]), Jiacai Yang (Investigation [Supporting]), Yong Huang (Investigation [Supporting]), Xiaohong Hu (Investigation [Supporting]), Cheng Chen (Investigation [Supporting]), Ruoyu Shang (Investigation [Supporting]), Wengang Hu (Investigation [Supporting]), Jue Wang (Investigation [Supporting]), Han-Ming Shen (Investigation [Supporting]), Jun Hu (Investigation [Supporting]), Gaoxing Luo (Validation [Lead]), and Weifeng He (Validation [Lead]).

Downloaded from academic.oup.com/burnstrauma/article/doi/10.1093/burnst/tkae071/8151405 by guest on 13 October 2026

Conflict of interest

None declared.

Funding

This study was supported by grants from the National Key Research and Development Program of China (Grant No. 2021YFA1101100) and the National Natural Science Foundation of China (Grant No. 82202464 and No. 82172232).

Data availability

All data are available from the corresponding author on reasonable request.

References

1. Eelen G, Treps L, Li X, Carmeliet P. Basic and therapeutic aspects of angiogenesis updated. *Circ Res* 2020;**127**:310–29. https://doi.org/10.1161/circresaha.120.316851.
2. Shpichka A, Butnaru D, Bezrukov EA, Sukhanov RB, Atala A, Burdukovskii V, *et al*. Skin tissue regeneration for burn injury. *Stem Cell Res Ther* 2019;**10**:94. https://doi.org/10.1186/s13287-019-1203-3.
3. Qin Q, Lee S, Patel N, Walden K, Gomez-Salazar M, Levi B, *et al*. Neurovascular coupling in bone regeneration. *Exp Mol Med* 2022;**54**:1844–9. https://doi.org/10.1038/s12276-022-00899-6.
4. Singer AJ, Clark RA. Cutaneous wound healing. *N Engl J Med* 1999;**341**:738–46. https://doi.org/10.1056/nejm199909023411006.
5. Augustin HG, Koh GY. Organotypic vasculature: from descriptive heterogeneity to functional pathophysiology. *Science (New York, NY)* 2017;**357**:eaal2379. https://doi.org/10.1126/science.aal2379.
6. Dudley AC, Griffioen AW. Pathological angiogenesis: mechanisms and therapeutic strategies. *Angiogenesis* 2023;**26**:313–47. https://doi.org/10.1007/s10456-023-09876-7.
7. Herbert SP, Stainier DY. Molecular control of endothelial cell behaviour during blood vessel morphogenesis. *Nat Rev Mol Cell Biol* 2011;**12**:551–64. https://doi.org/10.1038/nrm3176.
8. Ding BS, Nolan DJ, Butler JM, James D, Babazadeh AO, Rosenwaks Z, *et al*. Inductive angiocrine signals from sinusoidal endothelium are required for liver regeneration. *Nature* 2010;**468**:310–5. https://doi.org/10.1038/nature09493.
9. Brem H, Tomic-Canic M. Cellular and molecular basis of wound healing in diabetes. *J Clin Invest* 2007;**117**:1219–22. https://doi.org/10.1172/jci32169.
10. Geudens I, Gerhardt H. Coordinating cell behaviour during blood vessel formation. *Development (Cambridge, England)* 2011;**138**:4569–83. https://doi.org/10.1242/dev.062323.
11. Orecchia P, Conte R, Balza E, Petretto A, Mauri P, Mingari MC, *et al*. A novel human anti-syndecan-1 antibody inhibits vascular maturation and tumour growth in melanoma. *Eur J Cancer* 2013;**49**:2022–33. https://doi.org/10.1016/j.ejca.2012.12.019.
12. Kalluri R. Basement membranes: structure, assembly and role in tumour angiogenesis. *Nat Rev Cancer* 2003;**3**:422–33. https://doi.org/10.1038/nrc1094.
13. Tkach M, Théry C. Communication by extracellular vesicles: where we are and where we need to go. *Cell* 2016;**164**:1226–32. https://doi.org/10.1016/j.cell.2016.01.043.
14. György B, Szabó TG, Pásztói M, Pál Z, Misják P, Aradi B, *et al*. Membrane vesicles, current state-of-the-art: emerging role of extracellular vesicles. *Cell Mol Life Sci* 2011;**68**:2667–88. https://doi.org/10.1007/s00018-011-0689-3.
15. Maas SLN, Breakefield XO, Weaver AM. Extracellular vesicles: unique intercellular delivery vehicles. *Trends Cell Biol* 2017;**27**:172–88. https://doi.org/10.1016/j.tcb.2016.11.003.
16. Kalluri R, LeBleu VS. The biology, function, and biomedical applications of exosomes. *Science* 2020;**367**:367. https://doi.org/10.1126/science.aau6977.
17. Sheldon H, Heikamp E, Turley H, Dragovic R, Thomas P, Oon CE, *et al*. New mechanism for notch signaling to endothelium at a distance by Delta-like 4 incorporation into exosomes. *Blood* 2010;**116**:2385–94. https://doi.org/10.1182/blood-2009-08-239228.
18. Zhang X, Yuan X, Shi H, Wu L, Qian H, Xu W. Exosomes in cancer: small particle, big player. *J Hematol Oncol* 2015;**8**:83. https://doi.org/10.1186/s13045-015-0181-x.
19. Aliotta JM, Pereira M, Wen S, Dooner MS, del Tatto M, Papa E, *et al*. Exosomes induce and reverse monocrotaline-induced pulmonary hypertension in mice. *Cardiovasc Res* 2016;**110**:319–30. https://doi.org/10.1093/cvr/cvw054.
20. Stickney Z, Losacco J, McDevitt S, Zhang Z, Lu B. Development of exosome surface display technology in living human cells. *Biochem Biophys Res Commun* 2016;**472**:53–9. https://doi.org/10.1016/j.bbrc.2016.02.058.
21. Eming SA, Martin P, Tomic-Canic M. Wound repair and regeneration: mechanisms, signaling, and translation. *Sci Transl Med* 2014;**6**:265sr6. https://doi.org/10.1126/scitranslmed.3009337.
22. Li WW, Li VW, Hutnik M, Chiou AS. Tumor angiogenesis as a target for dietary cancer prevention. *J Oncol* 2012, **2012**:879623. https://doi.org/10.1155/2012/879623, 1, 23
23. Smith AN, Willis E, Chan VT, Muffley LA, Isik FF, Gibran NS, *et al*. Mesenchymal stem cells induce dermal fibroblast responses to injury. *Exp Cell Res* 2010;**316**:48–54. https://doi.org/10.1016/j.yexcr.2009.08.001.
24. Kachgal S, Putnam AJ. Mesenchymal stem cells from adipose and bone marrow promote angiogenesis via distinct cytokine and protease expression mechanisms. *Angiogenesis* 2011;**14**:47–59. https://doi.org/10.1007/s10456-010-9194-9.
25. Zhang Y, Hao Z, Wang P, Xia Y, Wu J, Xia D, *et al*. Exosomes from human umbilical cord mesenchymal stem cells enhance fracture healing through HIF-1α-mediated promotion of angiogenesis in a rat model of stabilized fracture. *Cell Prolif* 2019;**52**:e12570. https://doi.org/10.1111/cpr.12570.
26. Zhou Y, Zhang XL, Lu ST, Zhang NY, Zhang HJ, Zhang J, *et al*. Human adipose-derived mesenchymal stem cells-derived exosomes encapsulated in pluronic F127 hydrogel promote wound healing and regeneration. *Stem Cell Res Ther* 2022;**13**:407. https://doi.org/10.1186/s13287-022-02980-3.
27. Hu L, Wang J, Zhou X, Xiong Z, Zhao J, Yu R, *et al*. Exosomes derived from human adipose mensenchymal stem cells accelerates cutaneous wound healing via optimizing the characteristics of fibroblasts. *Sci Rep* 2016;**6**:32993. https://doi.org/10.1038/srep32993.
28. Shabbir A, Cox A, Rodriguez-Menocal L, Salgado M, Van Badiavas E. Mesenchymal stem cell exosomes induce proliferation and migration of normal and chronic wound fibroblasts, and enhance angiogenesis in vitro. *Stem Cells Dev* 2015;**24**:1635–47. https://doi.org/10.1089/scd.2014.0316.
29. Zhang J, Guan J, Niu X, Hu G, Guo S, Li Q, *et al*. Exosomes released from human induced pluripotent stem cells-derived MSCs facilitate cutaneous wound healing by promoting collagen synthesis and angiogenesis. *J Transl Med* 2015;**13**:49. https://doi.org/10.1186/s12967-015-0417-0.
30. Reinert RB, Brissova M, Shostak A, Pan FC, Poffenberger G, Cai Q, *et al*. Vascular endothelial growth factor-a and islet vascularization are necessary in developing, but not adult, pancreatic islets. *Diabetes* 2013;**62**:4154–64. https://doi.org/10.2337/db13-0071.
31. Veith AP, Henderson K, Spencer A, Sligar AD, Baker AB. Therapeutic strategies for enhancing angiogenesis in wound healing. *Adv Drug Deliv Rev* 2019;**146**:97–125. https://doi.org/10.1016/j.addr.2018.09.010.
32. De Lorenzi F, Hansen N, Theek B, Daware R, Motta A, Breuel S, *et al*. Engineering mesoscopic 3D tumor models with a self-organizing vascularized matrix. *Adv Mater* 2023;**36**:e2303196. https://doi.org/10.1002/adma.202303196.
33. Johnson LR, Lee DY, Eacret JS, Ye D, June CH, Minn AJ. The immunostimulatory RNA RN7SL1 enables CAR-T cells

Downloaded from academic.oup.com/burnstrauma/article/doi/10.1093/burnst/tkae071/8151405 by guest on 13 October 2026

to enhance autonomous and endogenous immune function. *Cell* 2021;**184**:4981–4995.e14. https://doi.org/10.1016/j.cell.2021.08.004.
34. Simons M, Gordon E, Claesson-Welsh L. Mechanisms and regulation of endothelial VEGF receptor signalling. *Nat Rev Mol Cell Biol* 2016;**17**:611–25. https://doi.org/10.1038/nrm.2016.87.
35. Olsson AK, Dimberg A, Kreuger J, Claesson-Welsh L. VEGF receptor signalling - in control of vascular function. *Nat Rev Mol Cell Biol* 2006;**7**:359–71. https://doi.org/10.1038/nrm1911.
36. Rey S, Semenza GL. Hypoxia-inducible factor-1-dependent mechanisms of vascularization and vascular remodelling. *Cardiovasc Res* 2010;**86**:236–42. https://doi.org/10.1093/cvr/cvq045.
37. Shi Y, Yang X, Xue X, Sun D, Cai P, Song Q, *et al.* HANR promotes lymphangiogenesis of hepatocellular carcinoma via secreting miR-296 exosome and regulating EAG1/VEGFA signaling in HDLEC cells. *J Cell Biochem* 2019;**120**:17699–708. https://doi.org/10.1002/jcb.29036.
38. Shou X, Wang Y, Jiang Q, Chen J, Liu Q. miR-126 promotes M1 to M2 macrophage phenotype switching via VEGFA and KLF4. *PeerJ* 2023;**11**:e15180. https://doi.org/10.7717/peerj.15180.
39. Xu L, Fu T, Wang Y, Ji N. Diagnostic value of peripheral blood miR-296 combined with vascular endothelial growth factor B on the degree of coronary artery stenosis in patients with coronary heart disease. *J Clin Ultrasound* 2023;**51**:520–9. https://doi.org/10.1002/jcu.23433.
40. Riazifar M, Mohammadi MR, Pone EJ, Yeri A, Lässer C, Segaliny AI, *et al.* Stem cell-derived exosomes as nanotherapeutics for autoimmune and neurodegenerative disorders. *ACS Nano* 2019;**13**:6670–88. https://doi.org/10.1021/acsnano.9b01004.
41. Babapoor-Farrokhran S, Qin Y, Flores-Bellver M, Niu Y, Bhutto IA, Aparicio-Domingo S, *et al.* Pathologic vs. protective roles of hypoxia-inducible factor 1 in RPE and photoreceptors in wet vs. dry age-related macular degeneration. *Proc Natl Acad Sci USA* 2023;**120**:e2302845120. https://doi.org/10.1073/pnas.2302845120.
42. Sagini K, Costanzi E, Emiliani C, Buratta S, Urbanelli L. Extracellular vesicles as conveyors of membrane-derived bioactive lipids in immune system. *Int J Mol Sci* 2018;**19**:19. https://doi.org/10.3390/ijms19041227.
43. Batrakova EV, Kim MS. Using exosomes, naturally-equipped nanocarriers, for drug delivery. *J Control Release* 2015;**219**:396–405. https://doi.org/10.1016/j.jconrel.2015.07.030.
44. Isaac R, Reis FCG, Ying W, Olefsky JM. Exosomes as mediators of intercellular crosstalk in metabolism. *Cell Metab* 2021;**33**:1744–62. https://doi.org/10.1016/j.cmet.2021.08.006.
45. Kalinec GM, Gao L, Cohn W, Whitelegge JP, Faull KF, Kalinec F. Extracellular vesicles from auditory cells as nanocarriers for anti-inflammatory drugs and pro-resolving mediators. *Front Cell Neurosci* 2019;**13**:530. https://doi.org/10.3389/fncel.2019.00530.
46. Lamichhane TN, Sokic S, Schardt JS, Raiker RS, Lin JW, Jay SM. Emerging roles for extracellular vesicles in tissue engineering and regenerative medicine. *Tissue Eng B Rev* 2015;**21**:45–54. https://doi.org/10.1089/ten.TEB.2014.0300.
47. Wilson SE. Corneal wound healing. *Exp Eye Res* 2020;**197**:108089. https://doi.org/10.1016/j.exer.2020.108089.
48. Davis GE, Kemp SS. Extracellular matrix regulation of vascular morphogenesis, maturation, and stabilization. *Cold Spring Harb Perspect Med* 2023;**13**:13. https://doi.org/10.1101/cshperspect.a041156.
49. Jandl K, Radic N, Zeder K, Kovacs G, Kwapiszewska G. Pulmonary vascular fibrosis in pulmonary hypertension - the role of the extracellular matrix as a therapeutic target. *Pharmacol Ther* 2023;**247**:108438. https://doi.org/10.1016/j.pharmthera.2023.108438.
50. Yang B, Chen Y, Shi J. Exosome biochemistry and advanced nanotechnology for next-generation theranostic platforms. *Adv Mater* 2019;**31**:e1802896. https://doi.org/10.1002/adma.201802896.
51. Mendt M, Kamerkar S, Sugimoto H, McAndrews KM, Wu CC, Gagea M, *et al.* Generation and testing of clinical-grade exosomes for pancreatic cancer. *JCI Insight* 2018;**3**:3. https://doi.org/10.1172/jci.insight.99263.
52. Thompson EM, Keir ST, Venkatraman T, Lascola C, Yeom KW, Nixon AB, *et al.* The role of angiogenesis in group 3 medulloblastoma pathogenesis and survival. *Neuro-Oncology* 2017;**19**:1217–27. https://doi.org/10.1093/neuonc/nox033.
53. Liu C, Yan X, Zhang Y, Yang M, Ma Y, Zhang Y, *et al.* Oral administration of turmeric-derived exosome-like nanovesicles with anti-inflammatory and pro-resolving bioactions for murine colitis therapy. *J Nanobiotechnol* 2022;**20**:206. https://doi.org/10.1186/s12951-022-01421-w.
54. Xu Y, Ouyang L, He L, Qu Y, Han Y, Duan D. Inhibition of exosomal miR-24-3p in diabetes restores angiogenesis and facilitates wound repair via targeting PIK3R3. *J Cell Mol Med* 2020;**24**:13789–803. https://doi.org/10.1111/jcmm.15958.

Downloaded from academic.oup.com/burnstrauma/article/doi/10.1093/burnst/tkae071/8151405 by guest on 13 October 2026

© The Author(s) 2025. Published by Oxford University Press. This is an Open Access article distributed under the terms of the Creative Commons Attribution Non-Commercial License (https://creativecommons.org/licenses/by-nc/4.0/), which permits non-commercial re-use, distribution, and reproduction in any medium, provided the original work is properly cited. For commercial re-use, please contact journals.permissions@oup.com
Burns & Trauma, 2025, 13, tkae071
https://doi.org/10.1093/burnst/tkae071
Research Article